Sensibility study for different nozzle configuration on the heat load and aerodynamic behaviour for the THEMIS demonstrator

Melissa Lantelme, Alexis Bourgoing, Charles Bertorello, Philipe Tran

Sensibility study for different nozzle configuration on the heat load and aerodynamic behaviour for the THEMIS demonstrator

LANTELME, Melissa[1]
[1] ONERA/DMPE, Université de Toulouse, 31055 Toulouse – France, melissa.lantelme@onera.fr

BOURGOING, Alexis[2]
BERTORELLO, Charles[2]
TRAN, Philippe[2]
[2] *Fluid Dynamics and Signatures Department, ArianeGroup SAS,* alexis.bourgoing@ariane.group
charles.bertorello@ariane.group, philippe.tran@ariane.group

Abstract

This paper's focus is on the aerodynamic and aerothermal loads that a reusable launch vehicle (RLV) during descent. The analysis is performed on a working design of the THEMIS demonstrator developed at Ariane Group SAS under an ESA contract. The paper describes the effects of parameters of the configuration of the nozzles. Impacts of these changes in shape on the aerothermal loads and the aerodynamic behaviour of the vehicle are addressed through the analysis of global aerodynamic coefficients and the static stability of the vehicles. Furthermore, the phenomena occurring in the flow field and its impacts on the heat flux distribution are investigated:

Acronyms/Abbreviations

AoA	Angle of Attack
AEDB	AErodynamic Data Base
ASCenSIon	Advancing Space Access Capabilities - Reusability and Multiple Satellite Injection
CALLISTO	Cooperative Action Leading to Launcher Innovation in Stage Toss-back Operations
CASCADES	Calculs Automatiques en Série des Coefficients Aérodynamiques d'Engins Spatiaux (Automatized Computations of Aerodynamic Coefficients of space vehicles)
CFD	Computational Fluid Dynamics
PROMETHEUS®	Precursor Reusable Oxygen METhane cost Effective propUlsion System
RANS	Reynolds Average Navier-Stokes
RLV	Reusable Launch Vehicle
THEMIS	Technologies for a Methane Innovative Stage

1 Context and objectives

This paper's focus is on the aerodynamic and aerothermal loads that a reusable launch vehicle (RLV) faces during different phases of their flight trajectory. The analysis is performed on a working design of the THEMIS demonstrator developed at ArianeGroup SAS under an ESA contract. THEMIS is planned to be a real scale demonstrator that is part of ESA's future launcher preparatory program and which will use the PROMETHEUS® engine currently being developed. It is designed as a vertical take-off vertical landing configuration and therefore relies on retropropulsion for deceleration and its maneuvers to reach its designated landing site. PROMETHEUS® investigates the possibility of a reusable 100-tons class LOx-LCH4 engine. The knowledge gained during CALLISTO and THEMIS will provide the information and experience required to determine the future of European operational launchers.

Within this paper, we will investigate different configurations of the three nozzles foreseen to be used for the THEMIS demonstrator. The presented sensitivity analysis focuses on the influence of the nozzle positions on the heat flux distribution and the overall aerodynamic behaviour and stability of the launcher. The paper aims to provide a determination of the best overall configuration minimizing the aerothermal loads. In order to determine this, trade-offs must be performed between the effects on different zones of the launcher (launcher's landing legs, base of the launcher; internal/external walls of the nozzles…) and the investigated physical properties. Impacts of these changes of shape are also addressed on the aerodynamic behaviour of the vehicle through the analysis of global aerodynamic coefficients (lift, drag) and the static stability of the vehicles (positions of centre of pressure).

The hereafter presented results were investigated within a collaborative effort between ArianeGroup SAS in Les Mureaux centre and ONERA Toulouse. This research is performed within the ASCenSIon project project funded by the European Commission (Horizon 2020).

2 Definition of test cases definitions, methodology and set-up

2.1 Configurations

The configurations presented hereafter are built especially for preliminary applications of the CASCADES code to an industrial case in advanced project phase and are not representative to the baseline of any projects in development.

The stage is composed of a fairing, a cylinder part of 3.45m diameter, four landing legs folded in this current configuration. The total length is about 31 m. In this study, neither duct lines nor covers are taken into account. The general dimensions of the vehicle (reference configuration) are shown in Figure 1.

The engine bay of the present configuration is constituted by three rocket engines in a linear alignment along the y-axis. A close-up in the vicinity of the engine bay is given in Figure 2.

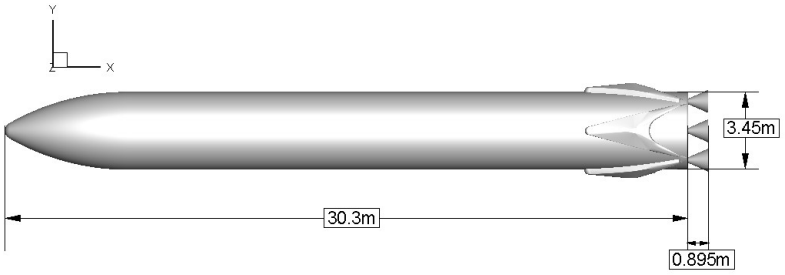

Figure 1: Reference Case: Main dimensions

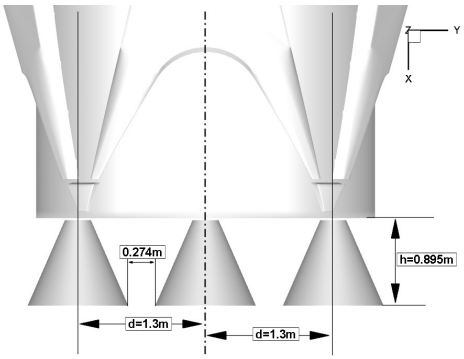

Figure 2: Geometry of the engine bay – reference case

2.2 Methodology and Tools

2.2.1 Tools

CASCADES is a set of tools which enables to compute an aerodynamic data base constituted by global aerodynamic coefficients of space vehicles like launchers on the basis of RANS CFD. This tool was initially developed for shape design in advanced project phases with the following main requirements:

- Quick time process
- Need of aerodynamic coefficients on huge range of Mach numbers, angles of attack; angles of sideslip
- Sensitivity of aerodynamics considering various shape design parameters
- Quick post-processing for aerodynamic analyses

Then CASCADES builds meshes, starts a matrix of computations and performs post-processing. CFD computations are executed within CASCADE with the in-house FLUSEPA solver. The flow solver FLUSEPA, developed by ARIANEGROUP, is a high order unstructured finite volume CFD code for the modelling of highly compressible, turbulent, viscous and reactive flows with particles over complex geometries in relative motion. Unlike the standard CHIMERA technique, FLUSEPA does not use interpolation methods, but an overlapping grids technique based on exact geometrical intersection. This conservative method avoids the loss of conservative variables at grids intersection due to interpolation. It consists of computing fluxes on the intersection surface between meshes [1] [2] [3].

2.2.2 Mesh generation process

The complete vehicle including the engines is meshed with a structured mesh and includes boundary layer refinements close to the surface. The inner part of the divergent of the nozzles has also treated with boundary layer refinement. The global refinement strategy is to split the flow domain into two sub-domains as depicted in Figure 3 (left). The domain 1 is coarse and covers the flow domain around the vehicle outside the engine bay. This flow in the engine bay is captured by the refinement of the domain 2. Mesh refinement in the vicinity of the engine bay is presented in Figure 3 (right). The height of the first cell in the boundary layer is set in the way to obtain a value y^+ of about one which is sufficient to ensure accurate heat fluxes.

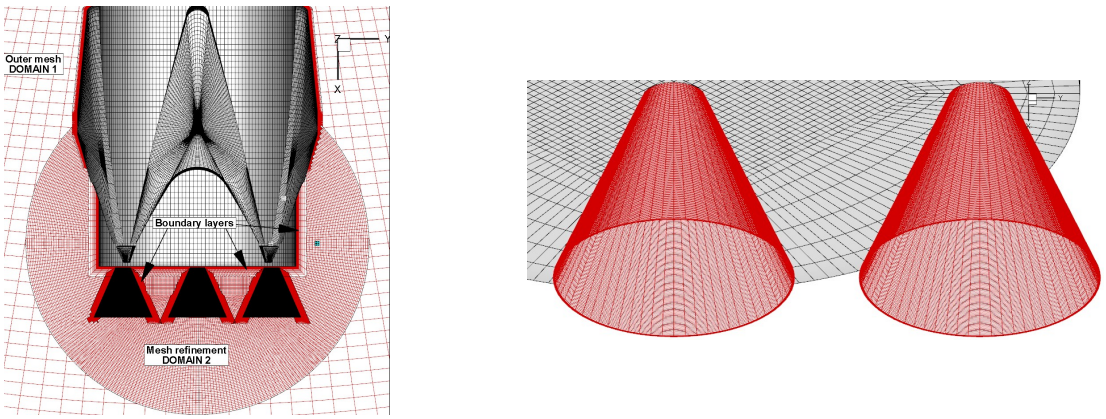

a. Overlapping grid strategy b. Mesh refinement in the engine bay

Figure 3: Mesh refinement

2.2.3 Boundary conditions and Flow modelling

All the computations presented in this paper were done at the same free stream conditions listed in Table 1. The wall temperature is uniform all along the vehicle and set to 300K. This fixed flight point is chosen to ensure significant aerothermal loads. All CFD calculations are performed for the controlled descent flight of the reusable THEMIS demonstrator in moments when the nozzles are not ignited. The gas is considered a perfect gas and the computations are done in turbulent regime using the k-ω SST Menter model. All the computations are done in steady mode.

Table 1: Free-stream and boundary conditions

Variables	Values	Units
Mach	4	-
Altitude	20	Km
Velocity	1180	m/s
Pressure	5670	Pa
Temperature	216	K
Wall temperature	300	K

2.3 Definition of the sensibility study

Within this paper, we will investigate different configurations of the three nozzles foreseen to be used for the THEMIS demonstrator. The sensitivity study presented in this paper is focused to the rocket engines aft-bay arrangement. The shape of the nozzles remains unchanged.

Table 2: Parameters of the investigated configurations

Configurations	h	d	δ	Number
Reference case	0.875 m	1.3 m	0°	#1
Vertical distance between nozzles	0.875 m	1.1 m	0°	#2
Gimballing outward	0.875 m	1.3 m	8.5°	#3
Gimballing inward	0.875 m	1.3 m	-5°	#4
Longitudinal nozzle position (maximum sinking)	0.29167 m	1.3 m	0°	#5
Longitudinal nozzle position (intermediate sinking)	0.5833 m	1.3 m	0°	#6

The changes studied are (see Figure 4 and Table 2):

- The distance *d* between the central nozzle and eccentrical nozzles,
- The extreme gimballing positions of the two off-centre nozzles on both side of the central one. The extreme values of the gimballing angle δ are chosen within the geometrical limits avoiding collisions of the nozzles
- The longitudinal emergence *h* of the three nozzles.

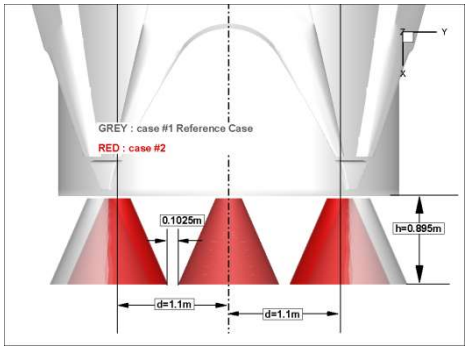

a. Configuration #2

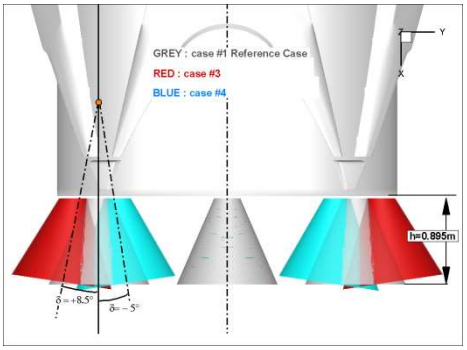

b. Configurations #3 and #4

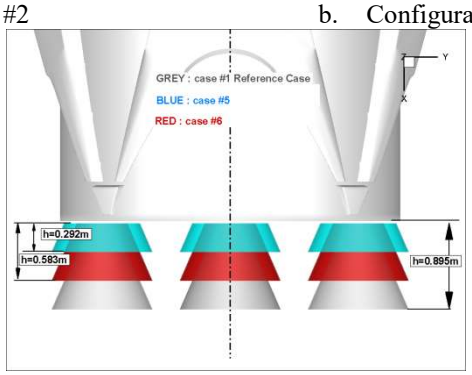

c. Configurations #5 and #6

Figure 4: Overview of the configurations

2.4 Aerodynamic coefficients

The orientation of the flow as well as the definition of the aerodynamic coefficients and the moment reduction centre position is depicted in Figure 5 (all the quantities are positive). The moment reduction centre (MRC) is set to the nose of the launcher.

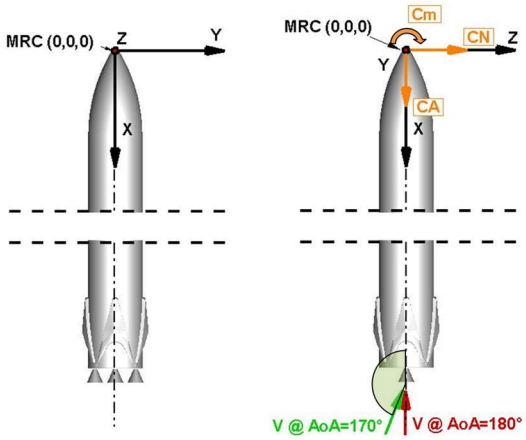

Figure 5: Aerodynamic axis reference frame

The following reference quantities are used to determine the force coefficients and moment coefficients:

- Reference surface: S_{ref}= 9.348m^2 (Surface of the circular section based on the diameter of the launcher)
- Reference length: L_{ref}=3.45m (diameter of the launcher)

The aerodynamic coefficients in the vehicle's axis system are the axial force coefficient CA, the normal force coefficient CN and the pitch moment coefficient Cm. The aerodynamic results presented hereafter are the drag coefficient CD, the lift coefficient CL given in the aerodynamic axis system (based on the free-stream velocity vector) and the centre of pressure X_{cp} expressed from the nose with the following formula [4]:

- $CD = cos(AoA).CA + sin(AoA).CN$ (1)
- $CL = -sin(AoA).CA + cos(AoA).CN$ (2)
- $Xcp = Lref.Cm/CN$ (3)

This configuration with nozzles of the engine bay encountering free-stream supersonic flow leads to an intrinsic unsteady aerothermo-dynamic flow field in the vicinity of the engine bay including part of the landing legs. It means that after a transient phase for which the CFD solution is established, the flow field still remains unsteady. Therefore, mean aerodynamic values are determined after this transient phase and presented with box plots showing the complete range of values (whiskers), the range lower to upper quartile values of the data (box) and the median of value with a line.

2.5 Heat flux

Heat flux distributions are plotted with the hereafter described methods permitting a good side-by-side comparison. Different zones of the launcher are investigated separately to focus on the different zones with different exposer levels independently. The wall distribution of heat fluxes are exported from CFD calculations at different instances and the time averaged value is determined for each cell of the mesh. The time-averaged value is determined by taking into account 30-50 exported instances. This number of exported time-steps has shown to converge to a reliable value.

Maximum values for different zones are compared between the different configurations in order to identify trends. The plots shown are created with two different methods. The first one is a circular plot, the second type displays the evolution of heat flux along the length of the launcher (section). For a specific area of the launcher (central core, landing legs, base plate, nozzle), respective angle of attack (170°, 175°, 180°) and nozzle configuration (see Table 1) all points on the surface of the launcher are preselected. For the circular plot, within this subsection for each angle θ (step 5°) the maximum value of heat flux for all points along x with this range in θ is determined and plotted in the, so called, circular plots as shown in Figure 6. Similarly, the longitudinal plots are created by searching for the maximum values on a cross-sections (all points for $\theta \in [0°,360°]$) for a specific section on the x-axis. The angle θ is defined in Figure 6 with θ=0° for z=0 and y>0 and θ=90° for y=0 and z>0.

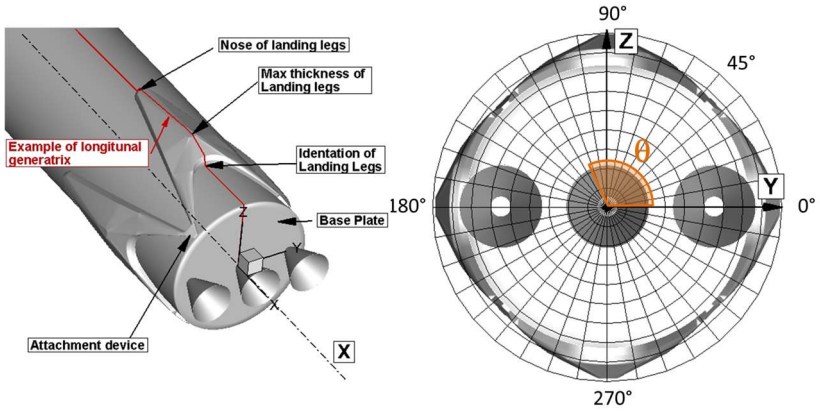

Figure 6: Visualization of the subset of data used for the circular (right) and longitudinal (left) plot

3 Aerodynamic Behaviour

3.1 Sensitivity to the distance between nozzles – Case #2

The main impact of bringing the two lateral nozzles closer to the central one (d=1.1) is a decrease in drag coeffient in absolute values as shown in Figure 7a for all AoA studied. It can furthermore be noted, that the drag is greatest for AoA=175°, which is an unexpected tendency. Indeed, usually the drag increases with increasing AoA. As expected, the lift coefficient (Figure 7b) is close to zero for an AoA=180° and increases with AoA.

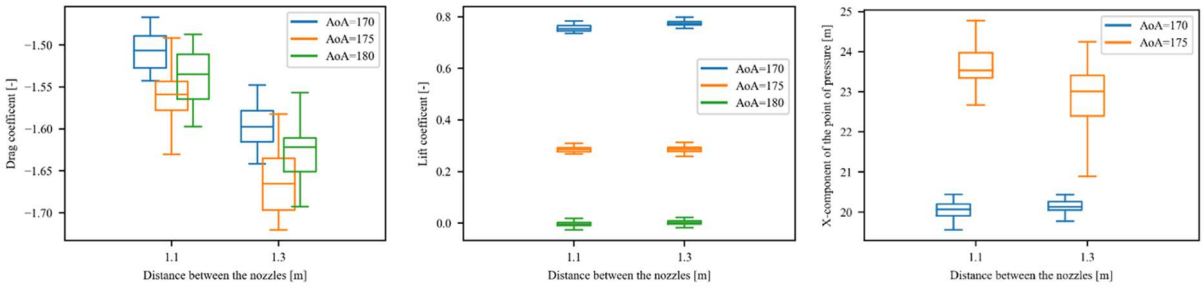

a. Drag coefficient CD b. Lift coefficient CL c. Centre of pressure X_{cp}

Figure 7: Influence of the lateral distance d on the aerodynamic properties (Case #2)

We observe an increase in lift very similar between the reference case and the case #2. As the majority of lift is provided by the central core and not the nozzles, the change in lift coefficient is negligible. The small observed changes in lift coefficient may be the result of numerical errors, and should therefore not be over- interpreted. The impact on the centre of pressure is also weak as depicted in Figure 7c. The main change of the location of X_{cp} is due to AoA. Note that the results are very scattered.

3.2 Sensitivity to the longitudinal nozzle position – Cases #5 and #6

The principal trend observed is an increase in drag coefficient for a decrease of longitudinal emergence *h* for all AoA studied. The differences between AoA=180° and AoA=175° are small, whereas the increase to an AoA of 170° has a significant effect on the drag coefficient for both cases #5 and #6 (Figure 8a). Note that at AoA=170°, the case #6 remains highly unsteady even after its transient phase regarding the aerodynamic forces and moments compared to the other cases. This results in a high margin of uncertainty or variability of the forces visualized with the large box plot. The effects on lift are small as already observed for the case #2 (Figure 8b). The impact on the center of pressure X_{cp} is a displacement towards the engine bay, which results in a destabilizing effect (Figure 8c).

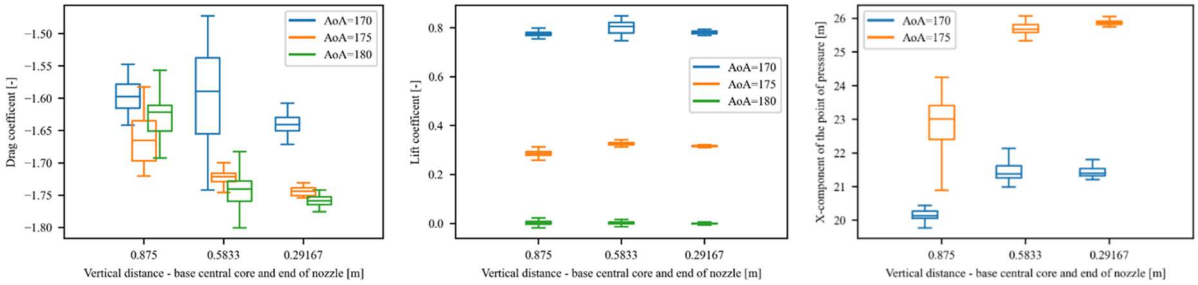

a. Drag coefficient CD b. Lift coefficient CL c. Centre of pressure X_{cp}

Figure 8 Influence of the longitudinal emergence *h* on the aerodynamic properties (Cases #5 and #6)

3.3 Sensitivity to the gimballing angle δ

The reference configuration is shown in the middle of the graphs in Figure 9. We observe a decrease in magnitude of the drag coefficient for negative gimballing angle δ (inward towards the central nozzle) and an increase for positive δ (outward rotation) compared to the reference configuration. Impact on lift coefficient is small. A negative gimballing angle δ has no effects on X_{cp} whereas positive gimballing induces the center of pressure to move towards the engine bay (destabilizing effects).

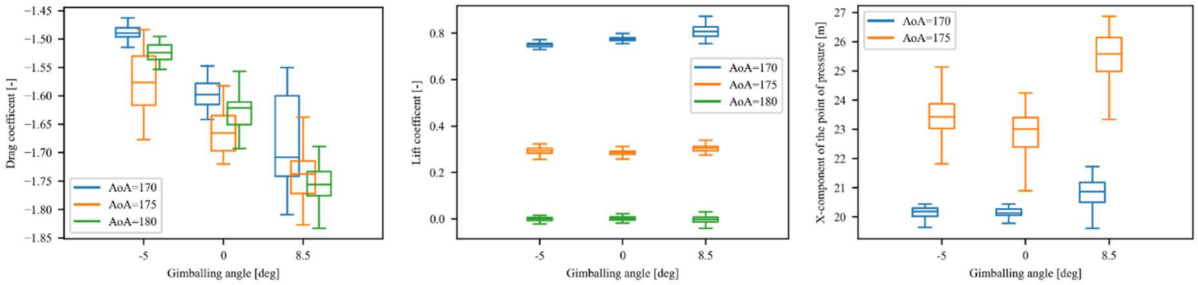

a. Drag coefficient CD b. Lift coefficient CL c. Centre of pressure X_{cp}

Figure 9: Influence of the gimballing angle δ on the aerodynamic properties (Cases #3 and #4)

4 Heat flux

4.1 General behaviour – Reference case

As already pointed out the flow around the launcher during descent is unsteady which leads to important fluctuations in heat flux, especially in the vicinity of the engine bay and landings legs. The shock is of symmetrical shape in the *X-Y* plane (see Figure 11) and non-symmetrical in the *X-Z* plane (see Figure 10) in case of an angle of attack out of the normal.The shape of the bow shock changes with the AoA, as expected, in the AoA plane (*X, Z*) but also locally in the plane perpendicular to *(X, Y)* Note that these images correspond to a fixed time step and the exact behaviour may change locally and with time. This behaviour is very different from the bow shock shape around a smooth spherical-like nose, which is usually steady in supersonic regime. Indeed, the flow between the bow shock and the base plate is

constituted by multiple recirculation zones due to the complex geometry of the engine bay (see Figure 10 and Figure 11).

Figure 12 shows, for three different time frames of the CFD calculation, the heat flux distribution for the reference case at AoA=180°. In general, the heat flux is high at the indentation of the feet and along the landing legs. We furthermore register a local increase in heat flux at the attachment point of landing legs. The base plate has a complex and non-homogeneous distribution of heat flux. There is no particular pattern in this area. Both on the internal and external wall of the three nozzles temporary and time averaged local increases in heat fluxes occur; furthermore, the edge of the nozzle is highly exposed to high heat fluxes.

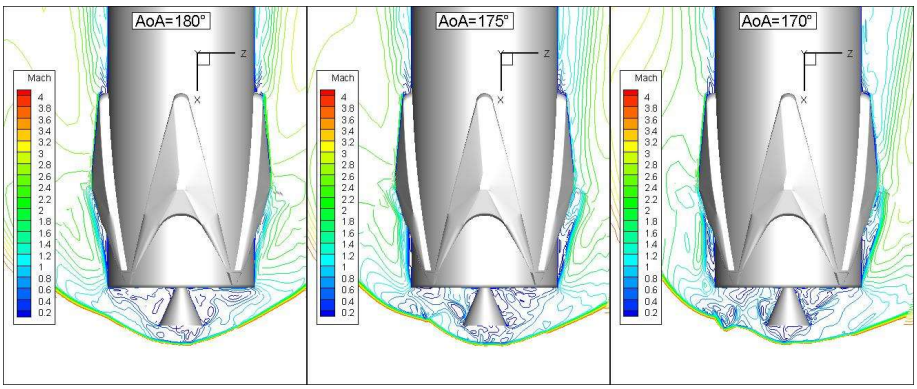

Figure 10: Mach distribution in the plane *(X; Z)* w.r.t AoA – Reference case

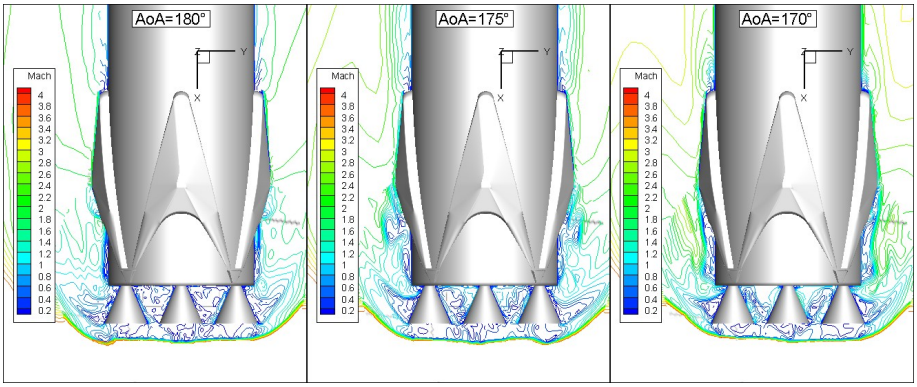

Figure 11: Mach distribution in the plane *(X; Y)* w.r.t AoA – Reference case

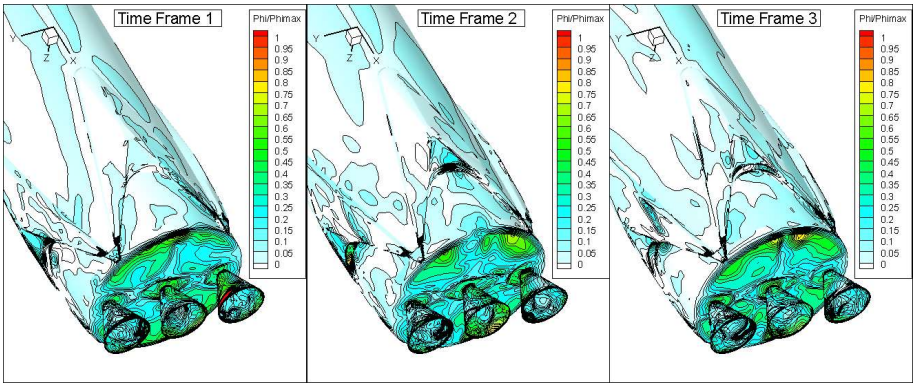

Figure 12: Dimensionless heat flux: reference case at AoA=180° at three time frames

The following sections analyse patterns and trends between the different configurations at the highly exposed regions (internal and external nozzle surface, base plate of the launcher, landing legs), which provide the basis for a recommendation regarding favourable configurations.

4.2 Central core and landing legs

4.2.1 Reference case #1

The maximum range of flux distribution along the x-axis on the central core is plotted in Figure 13a with a maximum of about 7.2· 10^5 W/m^2. The region of the landing legs experience great fluctuations due to an unsteady flow, whereas the heat flux determined on the remaining part of the central core does not experience strong changes. This maximum value is obtained in the vicinity of the attachment devices of the landing legs. Two secondary characteristic peaks are highlighted, at the nose of the feet and the second one close to the indentations and maximum thickness of the landing legs. Outside the landing legs area the heat fluxes are small (below 50 kW/m^2). The effects of AoA are weak and can be neglected.

The characteristic distribution of maximum values of the heat flux on the central core and landing legs along the circular distribution (along θ) w.r.t. AoA are not homogenous (see Figure 13 b). Maximum values are located at θ=45°, 135°, 225° and 315° corresponding to the location of the attachment devices. Others peaks, but smaller, are highlighted at θ=0°,180°, 90° and 270° corresponding to indentation of landing legs. Maximum values of heat fluxes are located, as expected, ahead of protrusions.

As expected for an AoA=180°, one observes an approximately symmetrical image between the windward side (y<0, $\theta \in$ [180°,360°]) and the leeward side (y>0, $\theta \in$ [0°,180°]), whereas an increase of AoA tends to reduce the characteristic heat flux peaks on the leeward side (z>0) but has a small effect on the windward side.

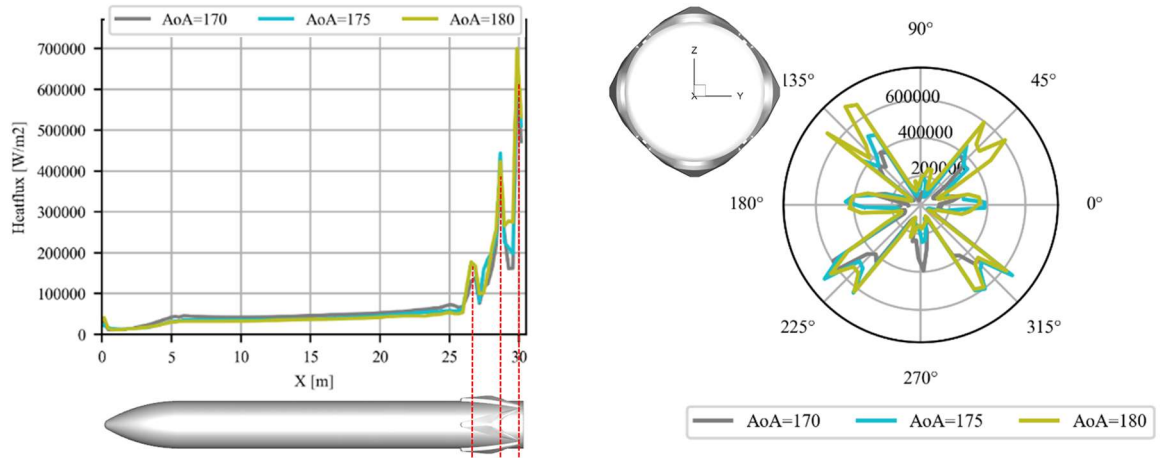

a. Along the x-axis b. Along the angle θ

Figure 13: Maximum heat flux [W/m^2] along $X \forall \theta$: (left) – Along $\theta \forall X$ – Reference case for different AoA

4.2.2 Influence of engine arrangement parameters

Since the area, having the maximum heat fluxes occurs at the attachment device of the landing legs, the maximum heat fluxes visible along θ in the circular plots correspond to the values found at that location. The effects of the different engine arrangements on the heat flux on the central core and landing feet is visualised in Figure 14 for AoA=175°.

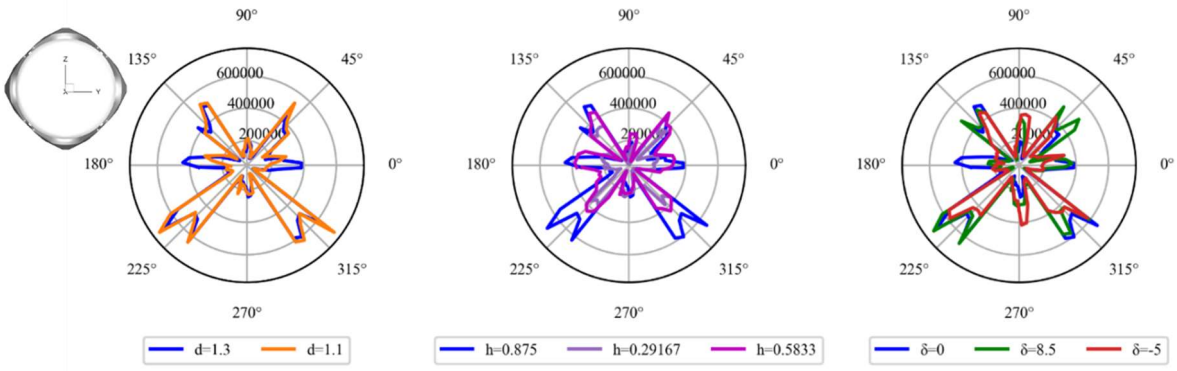

a. Cases #1 and #2 b. Cases #1, # 5 and #6 c. Cases #1, #3 and #4

Figure 14: Maximum heat flux [W/m^2] on the central core and landing legs for AoA=175° along θ (a-c)

A reduction of the vertical distance d (case #2) decreases the maximum heat fluxes at θ = 0° and 180°. This reduction is important because the maximum heat fluxes are almost divided by two (Figure 14 a). There is no other changes compared with reference case.

Changes in longitudinal nozzle position h tend to reduce heat fluxes on the windward side (θ = 225° and 315°) whereas on the leeward side, the results are inconclusive but show either a slight favourable trend or an insignificant increase depending on the AoA. The most important reduction is obtained for the maximum sinking of the nozzle (case #5). Note that for this case, heat fluxes in the windward side as well as in the leeward side are of the same magnitude (Figure 14 b).

The gimballing of the lateral nozzles outward or inward changes the heat fluxes distribution as depicted in Figure 14c). The gimballing inward (case #4) exhibits the same trends as the case #2 (reduction of the vertical distance d) which is coherent since this change tends also to reduce vertical distance of the nozzle. There is an exception to this trend, it concerns the heat fluxes at θ=90° and 270° where heat fluxes are above the reference case. The outward gimballing of the lateral nozzles (case #3) has same trends as case #4 on the windward side whereas the heat flux seems to be higher on the leeward side for an AoA=175°. Here again at θ =90° and 270° heat fluxes are above the reference case. At angles of the 0° and 180°, both gimballing inwards and outwards, results in a decrease in heat flux. Otherwise, outward gimballing does not show an overall beneficial change for all three angles of attacks studied (170°, 175°, 180°).

4.3 Base plate

The base plate experiences higher heat fluxes than the landing legs or the central core, as it represents the stagnation region of the THEMIS demonstrator together with the nozzles. On the base plate the overall range in time averaged heat flux is up to 6.4· 10^5 W/m^2 but local and temporary peaks can reach 8· 10^5-1· 10^6 W/m^2.

Analyses according to maximum heat flux distribution w.r.t. θ were done. The heat flux is strongly dominated by the unsteady characteristic of the flow and no pattern is easily identifiable regarding the location of peaks. This characteristic of the flow could explain why the distribution of time averaged heat flux along θ is not symmetric w.r.t. the symmetry plane *(X; Z)* for example for the reference case. Nevertheless, we want to highlight the main trends only and not a detailed description of heat fluxes distribution within this analysis. Figure 15 shows the influence of a variation in nozzle parameters on the angular distribution of heat flux on the baseplate for an angle of attack of 175°. Note that on the base plate heat fluxes on the windward side are below those of the leeward side (see Figure 15 a).

Reduction of the vertical distance d (case #2) globally reduces the maximum heat fluxes. This reduction slightly depends on the AoA. Depending on the angle of attack, we obverse a reduction in maximum value of up to -3% to –29%. At the angle of attack of 180°, the configuration with d=1.1 m shows an equal and locally (same θ value) increased magnitude in heat flux on the baseplate, which however remains below the maximum time-averaged value obtained on the base plate of the reference configuration.

Changes in longitudinal nozzle position tend to reduce the heat fluxes both on the windward and the leeward side (Figure 15 b). The most important reduction is obtained for the maximum sinking of the nozzle (case #5). We observe a reduction in maximum heat load by -33% to -47%, depending on the angle of attack. Here again, heat fluxes in the windward side are below those of the leeward side. However, it should be noted, that reducing the vertical distance h only to 2/3 of its initial length (h=0.588), does not show a clear trend of reduction in heat flux. Depending on the angle of attack, we may also observe an increase of up to 6% for the case of an angle of attack of 180°, or a reduction of overall maximum values of -23% and -35% for an angle of attack of 170° and 175° respectively.

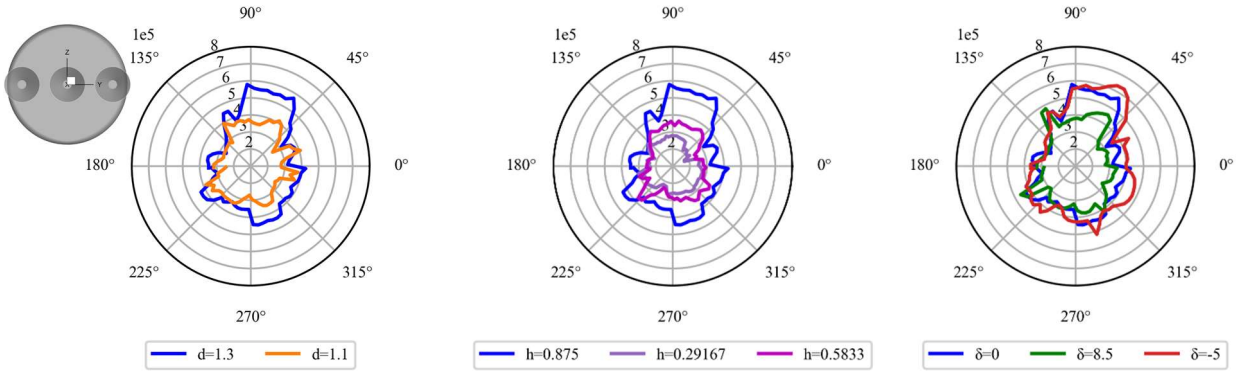

a. Cases #1 and #2 a. Cases #1, # 5 and #6 b. Cases #1, #3 and #4

Figure 15: Maximum time averaged heat flux [W/m^2] w.r.t. θ at AoA=175° - Base plate

The gimballing of the lateral nozzles inward by -5° (case #4) increases the maximum heat fluxes distribution slightly above the reference case for AoA= 175°, whereas for angles of attack of 170° and 180°, we observe a favourable change in heat flux in comparison to the reference configuration. An outward rotation shows a reduction in time averaged heat fluxes compared to the reference case on the baseplate for all studied angles of attack. If we compare the heat flux on the baseplate for different angles of attack for each configuration respectively, the intensity of the heat flux does not follow a trend.

4.4 Nozzles

The nozzles are the surfaces experiencing the highest time averaged heat flux can reach up to $1.2 \cdot 10^6$ W/m^2. The edges of the nozzles are highly exposed and experience important heat fluxes. The nozzles are subjected to high fluctuations and strong local temporary peaks, which makes it difficult to identify trends between geometrical changes, angles of attack or to compare the central to the lateral nozzles. One is occasionally capable to identify modes of multiple peaks, which move on the internal wall. Locally, both central and eccentric nozzles experience a negative heat flux at certain instances, as this is not a permanent phenomenon, it is not of major concern.

To study the distribution of the heat flux in the longitudinal direction of the nozzles, the maximum values of heat flux in the longitudinal direction on a circular section are determined and displayed in Figure 16 for the central nozzle. In general, on all nozzles, we see an increase in heat flux towards the edge of the nozzle and for some case a further increase towards the baseplate, as temporary peaks appear more frequently in those regions, the time-averaged heat flux captures this. Indeed, for the reference configuration depicted in Figure 16a there are no particular peaks but it enables to determine a range heat flux variations between 400kW/m^2 up to 900k W/m^2 for the central nozzle. Furthermore, the central nozzle experiences lower time-averaged heat fluxes than the lateral nozzles. This figure illustrates also exemplarily, that no trend between the angles of attack is visible. Furthermore, the external and internal wall have the same levels of heat flux and no clear trend between configurations at three angles of attack are observed.

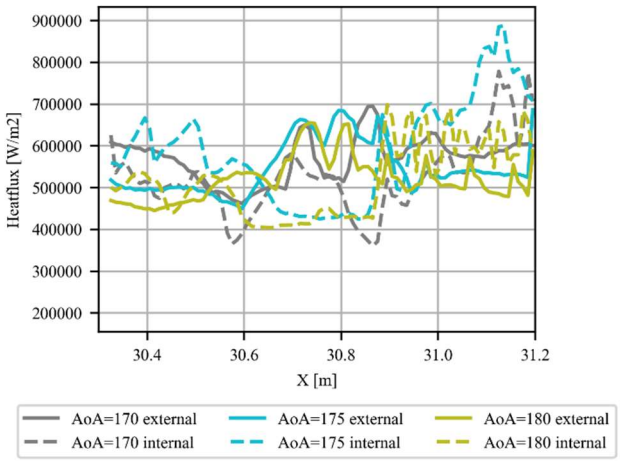

a. Reference cases #1 – Effects of AoA

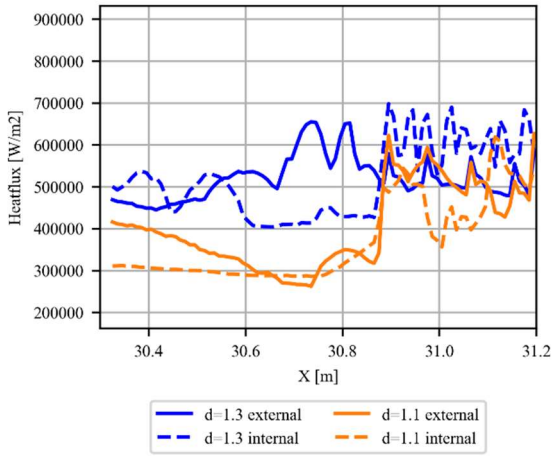

b. Cases #1 and #2

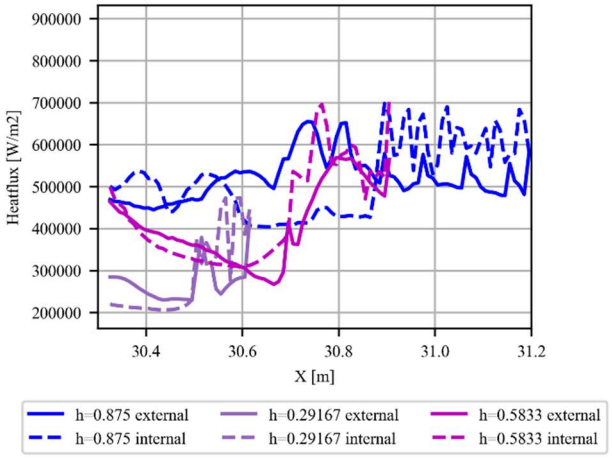

c. Cases #1, # 5 and #6

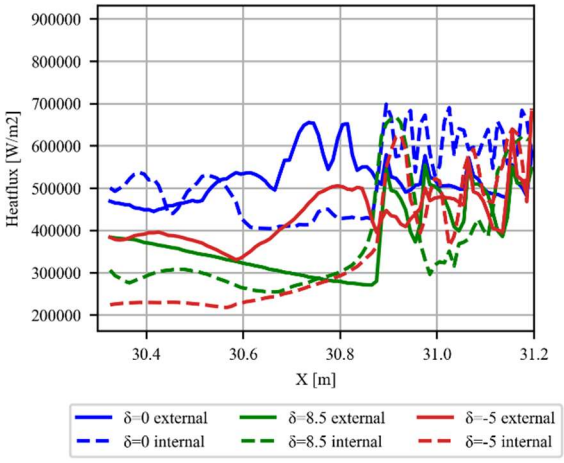

d. Cases #1, #3 and #4

Figure 16: Maximum time averaged heat flux [W/m^2] along the *X*-axis ∀ θ- Central Nozzle (b-d: at AoA of 180°)

The reduction of distance of lateral nozzles towards the central one (configuration #2) tends to reduce the heat flux on both internal and external wall, especially for area close to the base plate whereas area close to the nozzle's exit, heat flux remains in the same range of magnitude than the reference case (Figure 16b). However even if for most sections on the *X*-axis, on both lateral nozzles, the heat flux also decreases in comparison to the reference configuration, at some x-sections we register an increase in heat flux above the level of the reference configuration.

The same trends are also observed for an intermediate reduction of longitudinal nozzle position to h=0.58 m (case#6) as presented in Figure 16 c. The case #5 (maximum sinking to to h=0.29) results in an important decrease of heat flux on the internal and external wall for all angles of attack studied. At the edge of the nozzle, depending on the case (AoA, central/lateral nozzle), the maximum value in time-averaged heat flux at a specific section of the *X*-axis can extend the value found at the same section of the reference configuration. Nonetheless, compared to the value found at the edge of the reference configuration is remains below or at the same magnitude.

Inward gimballing by -5° results in a beneficial effect on the heat flux of the nozzle (Figure 16d). Depending on the case we observe similar or lower heat fluxes as the on the nozzle walls of the reference configuration. On the contrary, outward gimballing seems to hold a potential for a significant decrease in heat flux. However, this is only true for some of the studied cases in other cases; we observe a significant increase in heat flux resulting in an inconclusive tendency for this configuration.

An exhaustive analyses of time – averaged heat flux distribution along θ of the internal and external wall were done for all the configurations at the three AoA. On each of the three nozzles itself, no patterns of higher angular exposure along θ, is feasible for the totality of parameters studied. We expect to see higher heat fluxes along external walls of lateral nozzles facing the central nozzle. For some cases (configurations, AoA, nozzle), we see this expected pattern, in other cases this is not visible. An example of this pattern is shown for configurations #1, #5 and #6 presented in Figure 17 at AoA=180°(bold lines for the external walls). In these cases, one sees that for the reference case and case #6 external walls facing the central nozzle have the highest heat flux but it is not the maximum values since these maxima are obtains inside the nozzles. We can noticed that the important reductions of heat flux for the case #5 (maximum sinking) are also observed on lateral nozzles.

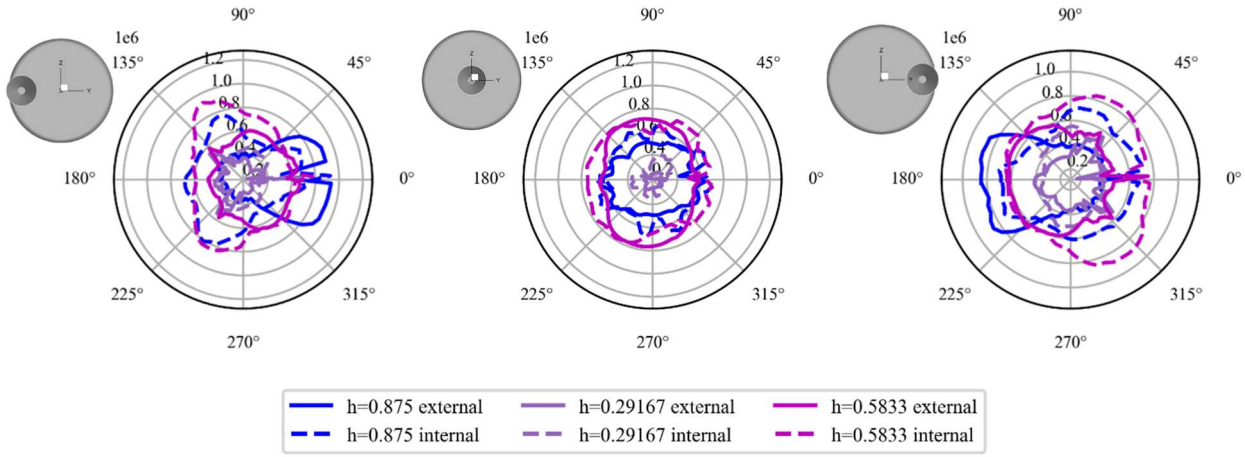

a. Eccentrical nozzle (center at y<0) b. Central nozzle c. Eccentrical nozzle (center at y>0)

Figure 17: Maximum time averaged heat flux on the internal and external wall the respective nozzle at AoA = 180° for configurations #1, #5, #6

5 Discussion

5.1 General organization of the flow

Figure 18 and Figure 19 illustrate that the different bay area configurations have different influences on the disturbance and recirculation zones of the flow and furthermore on the shape and position of the shock. Note that these images correspond to a fixed time step and the exact behaviour may change locally and with time.

5.1.1 Aerodynamics

The different cross sectional areas and size of the area disturbing the flow of the different nozzle configuration can explain the changes observed regarding the drag coefficient. This difference in cross sectional area underlines that the flow and shock are disturbed the greatest for the configuration with an outward gimballing angle for which we also observe the greatest magnitude in drag coefficient. The two configurations showing a reduction in the drag are the

configuration with reduced cross sectional area (inward rotation of the two eccentrical nozzles towards the central nozzle and the non-rotational displacement of the two eccentric nozzles towards the central nozzle).

5.1.2 Nozzles

As expected, the heat flux reaches higher magnitudes on the baseplate, the nozzles and the landing legs than on central core. The magnitude in maximum values in time averaged heat flux on the nozzles is higher than the levels obtained on the landing legs and baseplate, with the latter two experiencing similar thermal loads. Contrary to the aerodynamic coefficients, the engine arrangements have relevant consequences for the heat flux.

Heat flux peaks appear more often on the off-centre nozzles than on the central nozzle resulting in higher time-averaged heat fluxes. This difference may be due to the fact, that the central nozzle has a greater stock-stand off distance than the eccentric nozzles (see Figure 19), which are exposed to an oblique shock, which is closer to the nozzle edge and reduces the kinetic energy less than the perpendicular shock. Due to symmetry, the two eccentric nozzles do not show a significant difference in overall heat flux. The differences are to be explained by the unsteady behaviour of the flow. In the section of the nozzle closer to the baseplate, the internal wall often experiences lower heat fluxes, than the external wall. Toward the end of the nozzle, the thermal exposure of the internal wall reaches the same magnitudes of overtakes the levels of the external wall.

As described in section 4.4, we constituted the most reduced heat flux on the nozzles for the configuration with vertical distance h=0.29 m, whereas a reduction in horizontal distance d to 1.1 m, or in vertical distance h=0.58 m or gimballing internally, had either positive or no significant effects compared to the reference configuration. The heat fluxes are most likely due to the unsteady flow field with multiple recirculation zones (behind the nozzles, inside the nozzles). Those zones are reduced for the configuration with vertical distance h=0.29 m (see Figure 19e), but increased for the gimballing configurations (see Figure 19c/d). Furthermore the distance between the shock and the nozzles increases for a reduced distance h. Gimballing externally resulting in very mixed consequences of both increase and decrease, and are therefore not of interest for a selection of final configuration. This can be explained by the very complex and most disturbed flow field of case #3 (see Figure 18c and Figure 19c), where the shock is most uneven.

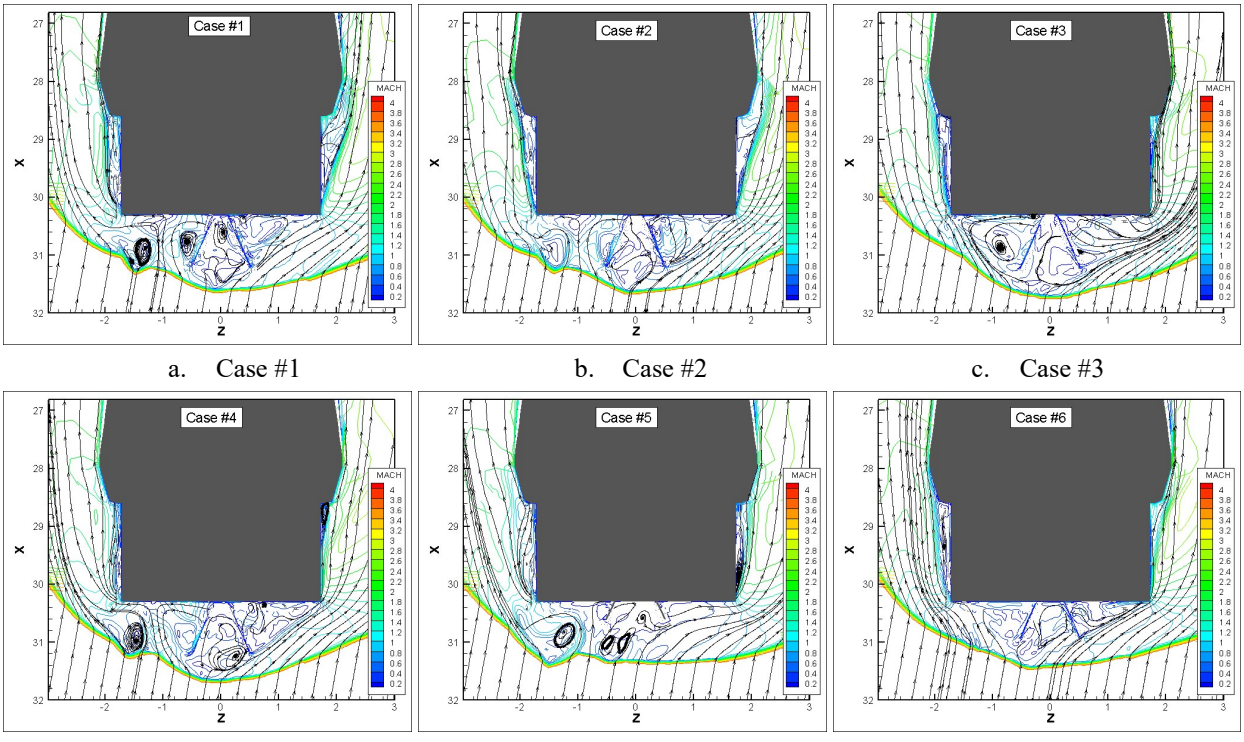

a. Case #1 b. Case #2 c. Case #3

d. Case #4 e. Case #5 f. Case #6

Figure 18: Organization of the Flow field – Engine bay – *(X, Y)* plane – AoA=170°

5.1.3 Landing legs

The nozzle parameters do not seem to have a big influence on the time-averaged heat flux on the central core and landing legs, expect for the indentations of the landing legs at θ = 0° and θ =180° (see Figure 14). As depending on the case, the heat fluxes at this position can reach levels, which are of the same magnitude as the ones obtained at the indentation on the windward side at θ = 270°, this might be a trend to consider.

Reducing the horizontal distance d has a protective effect on the indentations at θ = 0°/180°. Behind the nozzle, we observe zones of reduced velocity (Figure 19b), in the case of a reduced distance d, this slow speed zones causes a

slower flow around the corner resulting in a flow with less kinetic energy, which arrives at the indentations at θ = 0°/180° compared to the reference configuration.

As assumed one sees a beneficial effect on the landing legs at θ =0°/180° as the outward gimballed nozzles results in the fact that the landing legs are in the shadow of the nozzles (Figure 19c), however at other angles θ this configuration is not beneficial for the heat flux on the landing legs . Gimballing inwards results in a similar effect as reducing the distance *d*, which causes a low speed flow around the corner, resulting in an unchanged or decrease in maximum time averaged heat flux (Figure 19d). This is the only beneficial effect on the landing legs obtained by gimballing.

A reduction in vertical distance *h* of the nozzles shows a similar flow field at the landing legs as case#1 and seem to have beneficial effects only at θ =215°/315° (not visible in shown slices) of the landing legs, the other zones do not experience this favourable trend for all angles of attack, but neither shows an unfavourable behaviour.

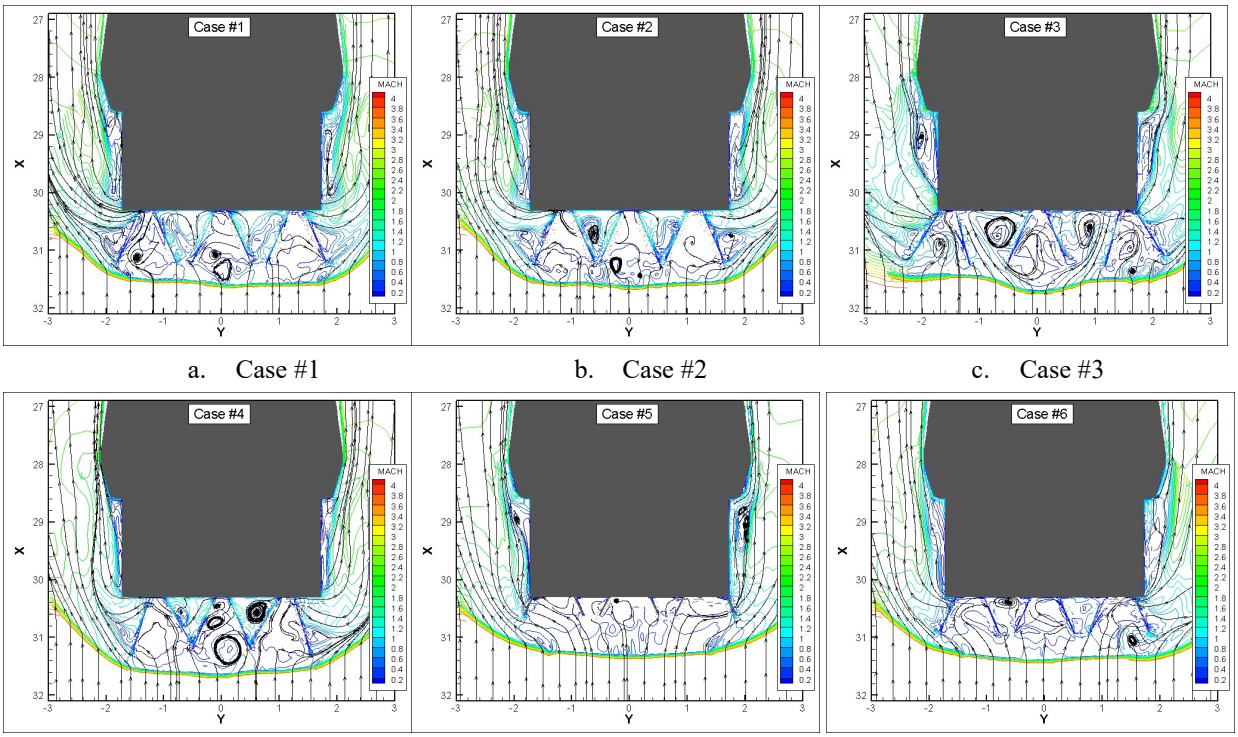

a. Case #1 b. Case #2 c. Case #3

d. Case #4 e. Case #5 f. Case #6

Figure 19: Organization of the Flow field – Engine bay – *(X, Z)* plane – AoA=170°

5.1.4 Base plate

The difference in heat flux on the baseplate can be explained by three causes, either the different shock shapes, the shock-stand-off distance or the beneficial effects due to the protective and shielding effects of the nozzles on the base plate or the combination of the three.

Inward gimballing angle δ and reducing the distance *d* to 1.1 m demonstrates an inconclusive effect on the heat flux on the base plate of the THEMIS demonstrator. As for some angles of attack, we obtain an increase in heat flux, further investigations are necessary to study this and evaluate if the increases are tolerable and if the reduction in time-averaged heat flux at the other angles of attack overall overweights the negative aspects. This is to be investigated in respect to the time periods of the return trajectory spend at the respective angles of attack. This similar result as seen for the reference configuration #1, can be explained by the similar flow field and shock shape (see Figure 18a/b/d and Figure 19 a/b/d).

We see beneficial effects on heat flux on the baseplate by reducing the vertical distance *h* (*h*=0,88 m , *h*=0,58 m, *h*=0,29 m) or for an outward gimballing by δ=8.5° . The most significant reduction in heat flux is seen for *h*=0,29 m. This can be the result of the fact that decreasing the distance *h*, results in less disturbance and recirculation zones, which decreases the heat flux on the base plate only for 0.29 m. The beneficial effects for outward gimballing are more likely due to different shielding effects, as the outward rotated nozzles may also increase the area on the baseplate which is not directly exposed to the freestream similar. This shielding effect is also visible in the angular distribution of the heat flux on the base plate (see Figure 15), where we observe a decrease in maximum heat flux on the horizontal axis (θ = 180° - 0°), where the nozzles are placed and higher heat fluxes on the vertical axis (θ =270°-90°).

A trend visible for all cases is the higher thermal loads experienced on the leeward side (θ =0°-180°) of the base plate, which is surprising, as the stock-stand-off distance on the windward side (θ =180°-360°) is smaller and fluctuates more

in position. However, the disturbance of the flow field which also affects the shock on the windward side for all configurations (see Figure 18) may explain this trend.

5.2 Synthesis

Table 3 shows a summary of the aerothermal trends observed on the different regions of the launcher for the different configurations, if the tendencies vary between different values of AoA or different sections, multiple tendencies are indicated.

All of the changes in configuration expect for outward gimballing, showed a decrease or similar thermal loads as the reference configuration on the landing legs and central core. However on the base plate only certain changes resulted in a decrease in heat flux (Configuration #5 with h=0.29 m), whereas other configurations experience similar or decreased levels (Configuration #6 with h=0.58 m, configuration #3 with δ=8.5°) or higher, lower or equal thermal loads (configuration #2 with d=1.1 m, configuration #4 with δ=-5°) depending on the angle of attack and region. On the nozzles, a recommendation can be given to configurations with a reduced vertical distance and inward gimballing (configuration #5 with h=0.29 m, configuration #6 with h=0.58 m, configuration #4 with δ=-5°). Whereas a reduction in horizontal distance and outward gimballing resulted in mixed results depending on the angle of attack and nozzle studied (Configuration #2 with d=1.1 m, configuration #3 with δ=8.5°). Therefore from an aerothermal perspective the configurations #5 and #6 should be further investigated with further values for the parameters h, to define a beneficial range of the parameter.

Table 3: Summary of the changes in aerothermodynamic properties with respect to the reference case#1

Configuration	Landing legs	Base plate	Nozzles
Case #2	Decrease/ no significant effect	Decrease/ no significant effect	Inconclusive (decrease/increase/ no effect)
Case #3	Increase	Decrease/ no significant effect	Inconclusive (decrease/increase/ no effect)
Case #4	Decrease/ no significant effect	Inconclusive (decrease/increase/ no effect)	Decrease/ no significant effect
Case #5	Decrease/ no significant effect	Decrease	Decrease/ no significant effect
Case #6	Decrease/ no significant effect	Decrease/ no significant effect	Decrease/ no significant effect

Table 4 summarizes the relevant aspects of the aerodynamic behaviour seen within this sensibility study. Regarding the aerodynamic behaviour, the lift remains unchanged by the changes in configuration, not allowing us to consider this aspect for the selection of beneficial configurations. The two selected parameters for further investigation (inward gimballing and reducing the vertical distance h) have different influences on the drag coefficient, whereas reducing the vertical distance h results in an increase in magnitude in drag, inward gimballing decreased the magnitude of drag. For propulsion, saving purposes during decent, further analysis is necessary to judge the favourable effect of a high drag configuration. However, the changes in aerodynamic coefficient seen though this study permits the conclusion that the studied configuration do not have a significant effect on the coefficients, and that the coefficients are more sensible to the AoA than the engine arrangement. Therefore the aerodynamic coefficients should not be the main driver for a decision regarding favourable configurations.

However, we observe that the nozzle positons play an important role in the stability of the launcher. Gimballing externally and reducing the longitudinal distance of the nozzles destabilises the launcher, whereas inward gimballing or a reduced distance d have either no significant or a destabilizing effect. These results are contraindicative and require further investigation, with the complete launcher design including the fins. Therefore the stability is an aspect to neglect for the purpose of this paper, as with the grid fins foreseen for the demonstrator the configurations should demonstrate a stable design.

Table 4: Summary of the changes in aerodynamic properties with respect to the reference case#1

Configuration	Drag coefficient	Lift coefficient	Aerodynamic stability
Case #2	Reduction	No significant change in respect to the reference configuration	Destabilised/ no significant change
Case #3	Increase		Destabilised
Case #4	Reduction		Destabilised/ no significant change
Case #5	Increase		Destabilised
Case #6	Increase		Destabilised

For a conclusion a reducing in horizontal distance *d* or a gimballing outwards, does not seem interesting for further investigations, unless the decrease in magnitude in drag is to be judged as a major decision driver for the nozzle configuration. In that case, the configurations with a reduced horizontal distance *d*, could also be considered, since the heat flux was mostly positively impacted. However, if a possible reduction in heat flux on the rear end of the launcher is of interest and the increase in magnitude in drag is justifiable, further analysis should be made for a reduction in vertical distance and inward gimballing.

6 Conclusion

Within this research, the influence of different parameters of the nozzle configurations on the aerodynamic coefficients and the aerothermal loads on the THEMIS demonstrator was studied. The main goals of this study were to assess impacts of nozzles arrangement inside the engine bay on the aerodynamic behavior as well as the heat flux distributions on the overall parts of the vehicle. These arrangements were limited to vertical and longitudinal positions as well gimballing angles of lateral nozzles.

The unsteady character of the flow occurring inside the shock layers is highlighted by and therefore the conclusions, which can be drawn between the configurations, must be taken with caution. However, a methodology was proposed to average heat flux distributions and aerodynamic coefficient, which permitted to identify preliminary trends. This method is not taking into account the unsteady behaviour and relying on simplifications. Nonetheless, it permitted to identify trends in a time-efficient manner. Furthermore, the reduction in dimension used to create the plots within this article seems reasonable and filters the relevant information for the predefined objectives of this study to minimize maximum heat flux values.

Regarding aerodynamics, there is no important effects on the drag and lift coefficients. The only main impact occurs on the center of pressure of longitudinal nozzle position changes (cases #5 and #6) which moves the X_{cp} towards the base plate of the engine bay compared to the reference case. Note that the AoA effects are also important regarding the X_{cp} position.

Regarding the heat fluxes, the maximum reduction of longitudinal position of the nozzle (case #5) and lesser for the intermediate reduction (case#6) reduce the heat flux for all the area examined (landing legs, base plate and nozzles), whether or not inward gimballing leads to a beneficial behavior required further calculations. Note that gimballing outward the nozzles (case#3) increases heat fluxes in the landing legs without any beneficial effects elsewhere.

Acknowledgments

The project leading to this application has received funding from the European Union's Horizon 2020 research and innovation programme under the Marie Skłodowska-Curie grant agreement No 860956.

References

[1] M. Pollet and P. Brenner. *Aerodynamics with moving bodies applied to solid propulsion*. AIAA paper 89-2779, 1989.

[2] P. Brenner. *A conservative overlapping grid to simulate rocket stage separation. 3rd Symposium on Overset Composite Grid and Solution Technology*. National Laboratory, New Mexico, USA, 1996.

[3] M. Bouarfa, A. Bourgoing, J-M. Carrat, D. Puech, M. Jubera, P. Brenner. *CFD retro-propulsion simulation with FLUSEPA code*. 56th 3AF International Conference on Applied Aerodynamics (*To be Published*)

[4] Anderson, J. D. 2001. *Fundamentals of aerodynamics*. Boston: McGraw-Hill.